Dai, C., Shum, C. K., Wang, R., Wang, L., Guo, J., Shang, K., Tapley, B. (2014): Improved constraints on seismic source parameters of the 2011 Tohoku earthquake from GRACE gravity and gravity gradient changes. - *Geophysical Research Letters*, *41*, 6, p. 1929-1936.

DOI: http://doi.org/10.1002/2013GL059178

AGU PUBLICATIONS

Geophysical Research Letters

RESEARCH LETTER
10.1002/2013GL059178

Key Points:
- Improved GRACE seismic signal retrieval
- Additional constraints on the 2011 Tohoku earthquake fault parameters
- GRACE produces unique slip rake angle, centroid location and seismic moment

Supporting Information:
- Readme
- Text S1
- Table S1
- Figure S1
- Figure S2
- Figure S3
- Figure S4
- Figure S5
- Figure S6
- Figure S7
- Figure S8
- Figure S9
- Figure S10
- Figure S11
- Figure S12
- Movie S1
- Movie S2
- Movie S3

Correspondence to:
C. Dai,
dai.56@buckeyemail.osu.edu

Citation:
Dai, C., C. K. Shum, R. Wang, L. Wang, J. Guo, K. Shang, and B. Tapley (2014), Improved constraints on seismic source parameters of the 2011 Tohoku earthquake from GRACE gravity and gravity gradient changes, *Geophys. Res. Lett.*, *41*, 1929–1936, doi:10.1002/2013GL059178.

Received 9 JAN 2014
Accepted 23 FEB 2014
Accepted article online 26 FEB 2014
Published online 19 MAR 2014

Improved constraints on seismic source parameters of the 2011 Tohoku earthquake from GRACE gravity and gravity gradient changes

Chunli Dai[1], C. K. Shum[1,2], Rongjiang Wang[3], Lei Wang[4], Junyi Guo[1], Kun Shang[1], and Byron Tapley[5]

[1]Division of Geodetic Science, School of Earth Sciences, Ohio State University, Columbus, Ohio, USA, [2]Institute of Geodesy and Geophysics, Chinese Academy of Sciences, Wuhan, China, [3]Physics of Earthquakes and Volcanoes, GFZ German Research Centre for Geosciences, Potsdam, Germany, [4]Division of Seismology, Geology, and Tectonophysics, Lamont-Doherty Earth Observatory, Columbia University, Palisades, New York, USA, [5]Center for Space Research, University of Texas at Austin, Texas, USA

Abstract A new approach of using only the *north* component of gravity change from Gravity Recovery and Climate Experiment (GRACE) data reveals that a substantially higher spatial resolution of the observed seismic deformation following the 2011 Tohoku earthquake is achievable at 333 km or longer. Here we show that GRACE-observed north component of gravity change, -17.6 ± 1.1 μGal, and the corresponding gravity gradient change, e.g., *Txz* at 1.25 ± 0.09 mEötvös, agree well with seismic/GPS model predictions. Localized Slepian spectrum analysis further confirms that the GRACE gravity and gravity gradient changes agree well with seismic model spectra and have powers up to the limit of the GRACE solution complete to spherical harmonic degree 60. Using the gravity observations for the fault parameter inversion via simulated annealing algorithm, we show that the estimated slip orientation and centroid location are different from GPS/seismic solutions and potentially due to the additional offshore constraint from GRACE data.

1. Introduction

The 11 March 2011 *Mw* 9.0 Tohoku earthquake ruptured the Okhotsk-Pacific interplate boundary of east Japan offshore up to about 40 m, with a fault area as large as 500×200 km^2 [e.g., *Ammon et al*., 2011; *Ozawa et al*., 2011; *Simons et al*., 2011]. Large postseismic slips [*Ozawa et al*., 2011] occurred with a moment of about 10% of the main shock. Several coseismic slip distribution models were determined using seismic data [*Hayes*, 2011; *Lay et al*., 2011; *Shao et al*., 2011]; Global Positioning System (GPS)-observed surface displacement data [*Ozawa et al*., 2011; *Pollitz et al*., 2011]; combined seismic and GPS data [*Wei et al*., 2012; *Ammon et al*., 2011]; and combined seismic, GPS, and tsunami data [*Simons et al*., 2011]. However, the estimated location and depth of the average slip d iffer significantly. Geodetic inversions give the average slip downdip [*Ozawa et al*., 2011; *Simons et al*., 2011; *Ammon et al*., 2011] of the Global Centroid Moment Tensor Project (GCMT) hypocenter (20 km depth) closer to land. Seismic inversions tend to give the average slip updip [*Shao et al*., 2011; *Hayes*, 2011; *Wei et al*., 2012], or even shallower near trench [*Lay et al*., 2011].

For earthquakes at ocean trenches, the near-source inland GPS and seismic stations, which are usually located at one side of the centroid, provide limited constraints on the rupture [*Wei et al*., 2012; *Lay et al*., 2011]. Since seismic inversions are highly dependent on the velocity structure [*Ji et al*., 2002], they have instabilities for shallow ruptures [*Lay et al*., 2011]. Surveying right above the rupture region over the ocean, although with a coarse spatial resolution at 333 km or longer, the data from Gravity Recovery and Climate Experiment (GRACE) twin-satellite mission have demonstrated the feasibility to detect and constrain focal mechanisms of large undersea earthquakes. A partial list of recent studies includes the 2004 Sumatra-Andaman earthquake [e.g., *Han et al*., 2006; *Wang et al*., 2012c; *Panet et al*., 2010], 2010 Maule, Chile earthquake [e.g., *Han et al*., 2010; *Heki and Matsuo*, 2010; *Wang et al*., 2012a], and the 2011 Tohoku earthquake [e.g., *Matsuo and Heki*, 2011; *Cambiotti and Sabadini*, 2012; *Han et al*., 2011, 2013; *Wang et al*., 2012b].

These coseismic deformation studies for large undersea earthquakes were demonstrated by using the inferred gravity gradient changes computed from GRACE temporal gravity field solutions, which resulted in spatial resolution enhancement and improved constraints for the 2004 Sumatra-Andaman earthquake [*Wang et al*., 2012c]. Other studies include spatial enhancement of the gravity change using Slepian basis functions

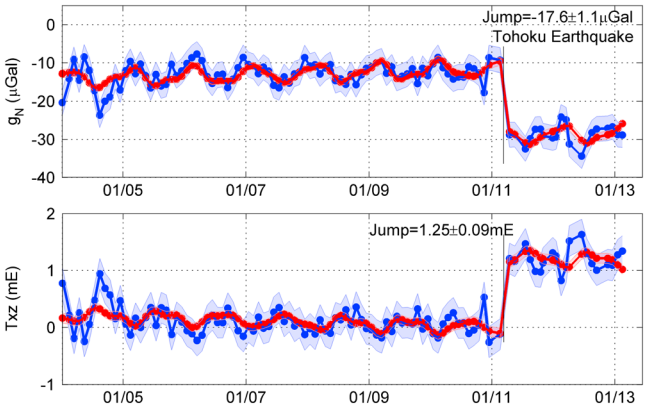

Figure 1. Time series of GRACE gravity and gravity gradient disturbances. Blue lines are the CSR RL05-derived gravity disturbance (top) g_N and the gravity gradient disturbance (bottom) *Txz* at the location of apparent maxima (139.6°E, 36.4°N, corresponding to white circles in Figures 2a and 3c). The uncertainties (blue shadings) are propagated based on the estimated a posteriori variance of unit weight for each coefficient. The red lines represent the model fits using equation (A1) in the supporting information including the estimated jumps at the earthquake occurrence.

[*Simons et al*., 2006] for the 2010 Maule, Chile earthquake [e.g., *Wang et al*., 2012a], and the direct processing of the intersatellite K band range (KBR) data and resolving for the seismic moment, dip angle, and rake angle based on normal mode formulation assuming point dislocation for the 2011 Tohoku earthquake [*Han et al*., 2011]. *Wang et al*. [2012a, 2012b] for the first time utilized Slepian functions to analyze GRACE-observed coseismic signals and developed a Markov Chain Monte Carlo algorithm to invert for fault length, width, and uniform slip of the 2010 Chilean Maule and the 2011 Tohoku earthquakes. Similar techniques were applied to the GRACE-observed 2011 Tohoku earthquake seismic signals and source parameter inversion by *Cambiotti and Sabadini* [2012]. *Wang et al*. [2012c] first demonstrated that the correlated errors in the GRACE temporal gravity field solution can be substantially suppressed using the *Txx* and *Txz* (*x* and *z* refer to north and up directions, respectively) components of gravity gradient change. *Li and Shen* [2011] also conducted a study on the Sumatra earthquake and addressed only the *Txz* component. Fault parameter inversions using GRACE data based on multiple centroid moment tensors and normal mode formulation have been demonstrated for a number of large earthquakes over the last decade [*Han et al*., 2013].

In this paper, a new approach for GRACE data processing using only the *north* component of the observed gravity change and the corresponding gravity gradient change is described and applied to the 2011 Tohoku earthquake. As a result, no decorrelation or spatial filtering of the GRACE data is needed, leading to improved spatial resolution at the full wavelength corresponding to spherical harmonics complete to degree 60. The resulting gravity change data are then used in an inversion scheme to estimate the fault parameters including the seismic moment, fault length, width, rake angle, and the centroid location. We then conduct sensitivity analysis to quantify the unique contribution of GRACE as compared to GPS/seismic data estimated slip models in constraining the fault parameters for the 2011 Tohoku earthquake.

2. GRACE Data Analysis

GRACE L2 Release 05 (RL05) monthly geopotential solutions complete to degree 60 are used to generate the disturbing potential by subtracting a reference model (GOCO02S), from January 2004 to February 2013. The L2 data products from the University of Texas Center for Space Research (CSR), Deutsches GeoForschungsZentrum (GFZ) German Research Centre for Geosciences, and Jet Propulsion Laboratory (JPL) are analyzed (supporting information). Here we choose to present the results using the CSR L2 data products. Three components of gravity disturbance, g_N, g_E, and g_D, are the first derivatives of the disturbing gravitational potential, *T*, in the local north-east-down directions, respectively. The gravity gradient disturbances, *Txx*, *Txy*, *Txz*, *Tyy*, *Tyz*, and *Tzz* (*y* axis is west direction), are the second derivatives of *T*. We then conduct an analysis of the gravity and gravity gradient disturbance time series over the 0.4° by 0.4° gridded study region.

Figure 1 shows the gravity (north component or g_N (Figure 1, top)) and gravity gradient (*Txz* (Figure 1, bottom)) disturbance time series (blue lines) from January 2004 through February 2013 (excluding March 2011) at a selected location with maximum jump. *Txz* represents the largest gravity gradient component. The uncertainties (blue shading) are propagated based on the estimated a posteriori variance of unit weight for each coefficient. In order to isolate the earthquake seismic deformation signal, periodicities associated with

the annual, semiannual, and the 161 day S_1 tidal aliasing periods [*Wang et al*., 2012a, 2012b] are simultaneously fitted with a linear trend and the Heaviside step function for the jump at the earthquake epoch (equation (A1) in the supporting information) for each time series. Figure 1 shows that the annual signal dominates both time series. At the earthquake epoch, g_N (Figure 1 (top)) decreases significantly, with the estimated earthquake-triggered jump as -17.6 ± 1.1 μGal. For *Txz* (Figure 1 (bottom)), the estimated jump is also substantial at 1.25 ± 0.09 mEötvös (mE). We find that the approach using Heaviside step function can better reveal the seismic gravity and gravity gradient change, and less contaminated by the long-term viscoelastic postseismic signal.

For GRACE L2 data postprocessing, destriping, or decorrection technique is widely used to remove or reduce the high-frequency correlated errors in GRACE temporal gravity field solutions [e.g., *Swenson and Wahr*, 2006; *Duan et al*., 2009]. However, the decorrelation process may partially eliminate the seismic gravity change signal [*Wang et al*., 2012a, 2012c] and/or alter the orientation of the spatial pattern, which is the key observation to constrain the dislocation vector orientation. Although Gaussian smoothing can reduce the ripple effects caused by the band-limited L2 solution, as a low-pass filter it also could smooth out or diminish the desired earthquake-induced high-frequency signal. As shown in the next section, our approach using the north component of gravity and the corresponding gravity gradient change can effectively avoid the contamination by the north-south stripes; hence, it can better preserve the seismic signal by avoiding the negative effect from destriping and Gaussian smoothing.

3. Comparison Between GRACE-Derived and Model-Predicted Gravity Change

The coseismic slip distribution model generated using teleseismic body waves and near-source GPS observations [*Wei et al*., 2012] and the postseismic slip distribution model produced using GPS displacement data for 12–25 March 2011 [*Ozawa et al*., 2011] are adopted to compute gravity and gravity gradient changes. Here we use the PSGRN/PSCMP software [*Wang et al*., 2006], based on the 1-D velocity model [*Wei et al*., 2012], with the top replaced by an ocean layer extracted from the bathymetry data in CRUST2.0 model [*Bassin et al*., 2000] and account for the effect of ocean water displacement. As the fault dislocation is undersea, the passive response of the ocean water is considered, which reduces about 40% of the gravity change due to the solid Earth deformation (Figure S4 in the supporting information). Gravity change at the ocean floor due to both solid Earth deformation and the passive response of ocean water is upward continued to Earth's surface (Figure S5 (right)), truncated to spherical harmonic degree 60 (Figures 2d–2f) to be consistent with GRACE solution. The observed and the modeled gravity change are then transformed to all components of gravity and the corresponding gravity gradient changes, and compared in both spatial and spectral domains.

3.1. Comparison in Spatial Domain

The GRACE-observed and model-predicted gravity and gravity gradient changes corresponding to the 2011 Tohoku earthquake are compared with a resolution commensurate with the GRACE observations. For the GRACE-derived g_N change (Figure 2a), the positive-negative-positive pattern is evident and agrees well with model predictions (Figure 2d). The GRACE-observed g_N change is substantial and reaches -17.6 ± 1.1 μGal at 139.6°E, 36.4°N (Figure 4a), with the magnitude slightly greater than the model prediction, -13.6 μGal. The profile along 140.4°E (Figure 4a) also shows good agreement between observed and model-predicted g_N, with GRACE-observed magnitude slightly larger than the prediction. The spatial patterns of the GRACE-observed g_N (Figure 2a) are found to be at an orientation of about 10° clockwise of the model-predicted g_N orientation (Figure 2d, Movie S1), which implies that a different slip vector direction (e.g., rake angle) is preferred by GRACE data.

It is evident that larger stripes exist in the GRACE-derived g_E, g_D changes. For the g_E change, although the negative-positive-negative pattern centered over the Tohoku region (Figure 2b) is visibly similar to the model prediction (Figure 2e), the surrounding error is too large to clearly isolate the seismic-induced signal. Analogous to the g_E change, the surrounding error for the g_D change (Figure 2c) is also too large. From the GRACE observation, the north-south stripes occur in g_E, g_D changes, because the KBR measurement is highly sensitive to g_N change but relatively insensitive to g_E, g_D changes because of the near 90° orbital inclination. Theoretically speaking, since $g_N = -\partial T/\partial\theta/r$, the g_N change obviously has diminished north-south stripes where the disturbing potential is differentiated along the meridian direction. This is the same for the gravity

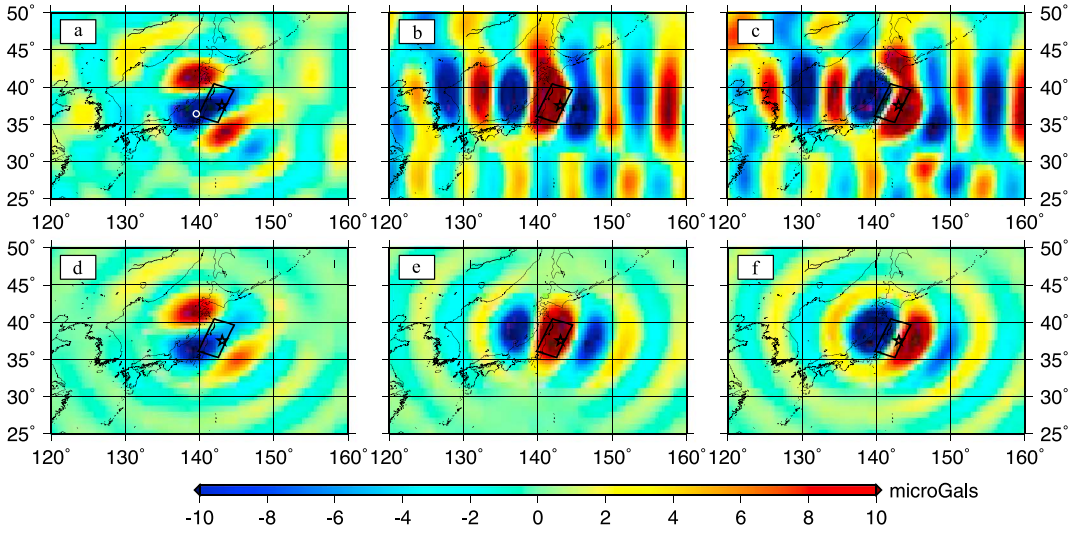

Figure 2. Comparison of GRACE-observed and model-predicted coseismic and postseismic (March 2011) gravity changes. GRACE-observed (a) g_N, (b) g_E, and (c) g_D changes are compared to the coseismic and postseismic model-predicted (d) g_N, (e) g_E, and (f) g_D changes, respectively. The uncertainties for observed g_N, g_E, and g_D changes are approximately 1.2, 2.5, and 2.8 μGal, respectively. The white circle in Figure 2a is the location of maxima to show the time series in Figure 1. The black rectangle is the coseismic fault plane boundary, and the black star is the Global Centroid Moment Tensor Project (GCMT) centroid (143.05°E, 37.52°N) (http://earthquake.usgs.gov/earthquakes/eqinthenews/2011/usc0001xgp/neic_c0001xgp_gcmt.php).

gradient observables, only north associated components of gravity gradient changes have reduced stripes or correlated errors. The other three components, *Tyy*, *Tyz*, and *Tzz*, like g_E, g_D, are basically contaminated by high-frequency correlated error, which is twice of that for the *Txx*, *Txy*, and *Txz* components.

The GRACE-observed gravity gradient change is shown in Figure 3. For the *Txx* change (Figure 3a), the main negative-positive-negative-positive pattern distributed from Sea of Japan to southeast coast of Kanto matches well with the model prediction (Figure 3d). The surrounding positive-negative ripple effect is even mimicking the predicted ripple effect in Figure 3d. For the *Txy* change (Figure 3b), the main negative-positive pattern is also similar with the prediction (Figure 3e), even with the analogous "8" shape positive pattern. The *Txz* change (Figure 3c) matches the prediction as well, with the maximum change of 1.25 ± 0.09 mE at

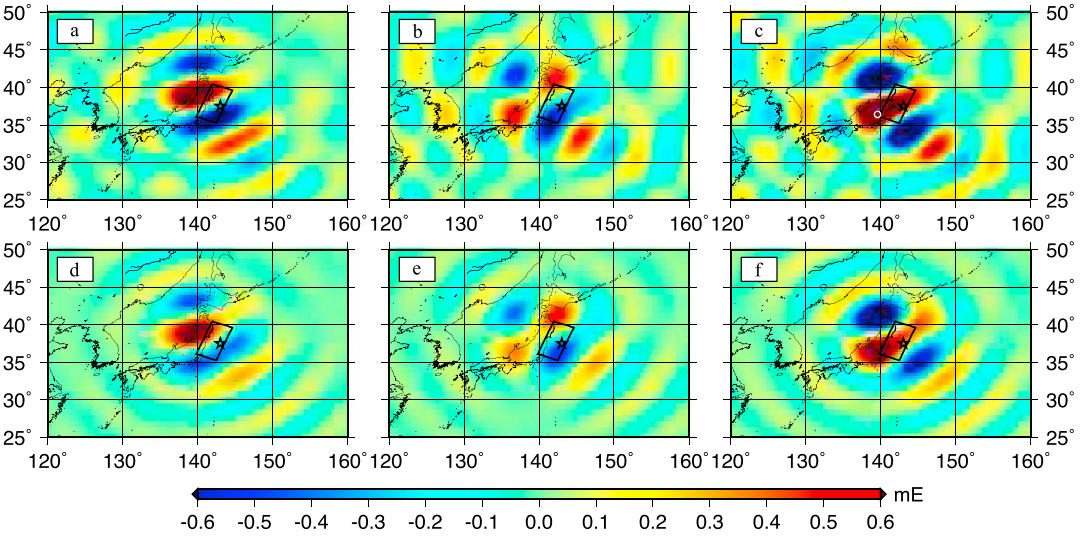

Figure 3. Comparison of GRACE-produced and model-predicted gravity gradient change. GRACE-produced (a) *Txx*, (b) *Txy*, and (c) *Txz* changes. Coseismic and postseismic model-predicted gravity gradient changes: (d) *Txx*, (e) *Txy*, and (f) *Txz*. Other descriptions are the same as in Figure 2.

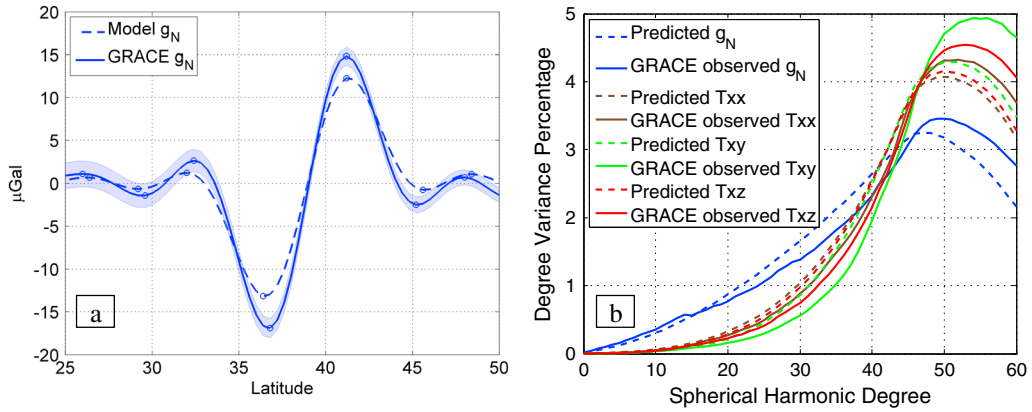

Figure 4. Comparison in the spectral domain and along a profile. (a) Model-predicted and GRACE-observed north component of gravity change g_N along the profile of 140.4°E. Shading denotes the estimated standard deviation. (b) Percentage of the degree variance as a function of spherical harmonic degree, for observed and model-predicted north component of gravity change, g_N, and the corresponding gravity gradient changes, *Txx*, *Txy*, and *Txz*.

139.6°E, 36.4°N, slightly larger than the prediction, 0.95 mE. Coincide with the orientation of the spatial pattern of g_N in Figure 2a, GRACE-observed gravity gradient change (Figure 3) precedes about 10° clockwise of the model-predicted g_N orientation.

3.2. Comparison in the Spectral Domain

To compare the spectrum of the earthquake-induced gravity and gravity gradient changes, the localized spectral estimates are carried out using Slepian tapering windows [*Wieczorek and Simons*, 2005] centered at the 2011 Tohoku earthquake centroid. Figure 4b presents the percentage of the degree variance of the observed and model-predicted g_N, *Txx*, *Txy*, and *Txz* changes in the study region, showing the consistency between the observed and the model-predicted values. It shows that both gravity and the corresponding gravity gradient changes are dominated by the higher-degree signals. Consistent with *Wang et al.*'s [2012c] conclusion for the 2004 Sumatra-Andaman earthquake, Figure 4b validates that gravity gradient changes have relatively high power for degrees above 42, about 25% greater than the g_N change. Although gravity gradient can enhance the high-frequency details, they are noisier, as demonstrated by their unexpected higher power for degrees above 48, especially for *Txy*, which contains the term T_λ (partial derivative of *T* with respect to longitude), contaminated by the south-north stripes. The power percentage of *Txx*, *Txy*, and *Txz* for degrees above 48 are larger than the prediction for about 4.5, 9, and 6.5, respectively, whereas the fractional misfit for g_N is less than that for *Txy* and *Txz* but more than that for *Txx*. The JPL GRACE solution-derived degree variance (Figure S6) further illustrates that g_N has the lowest noise level compared to all other components of gravity and gravity gradient changes.

4. Inversion of Fault Parameters Using GRACE Data

To demonstrate the sensitivity of GRACE-observed north components of gravity and its corresponding gravity gradient changes to seven fault parameters, numerous synthetic scenarios have been carried out (Figures S7–S11). These figures show that the spatial orientation of gravity and gravity gradient change rotates in the same direction as either strike or rake angle changes, agreeing with *Han et al.*'s [2011] conclusion that there is a monotonic relationship between gravity change pattern and strike and rake angles. Since the strike angle is well constrained by other kinds of data, such as the aftershocks area, and the plate boundary direction, we fixed the strike angle during our inversion. As a result, the rake angle can be effectively constrained by GRACE observations. In addition, the dislocation magnitude and fault width are highly sensitive to the gravity signal. Since there is a trade-off between the fault width, dip angle, and fault depth, and as the GRACE-observed signal is least sensitive to fault depth and most sensitive to fault width, the fault width can be resolved during the inversion while fixing the fault dip angle and depth (Table 1).

Using the simulated annealing algorithm [*Kirkpatrick et al.*, 1983; *Goffee et al.*, 1994] and an approach similar to *Wang et al.* [2012a] but for a different earthquake, the rake angle, fault location, width, and uniform or

Table 1. Comparison of Fault Parameters

Model	Data Source	Rake Angle (deg)			Strike Angle (deg)			Dip (deg)	Seismic Moment (N m)
		Min	Max	Average	Min	Max	Average	Average	
Ozawa et al. [2011]	GPS	72	107	87	181	217	196	11	3.43×10^{22}
Wei et al. [2012]	GPS and seismic data	70	110	89		201[a]		10[a]	5.31×10^{22a}
GCMT	Long-period mantle waves		88			203		10	5.31×10^{22}
USGS CMT	Seismic data		68			187		14	4.50×10^{22}
Han et al. [2011]	GRACE Release 01 KBR data		82			196[a]		10.5	5.40×10^{22}
This study	GRACE CSR RL05 data		77.0 ± 2			201[a]		10[a]	$6.43 \pm 0.4 \times 10^{22}$

[a]Parameter fixed during inversion.

average slip magnitude have been resolved with strike angle fixed at 201°, fault dip angle fixed at 10°, and the depth of the top edge of the fault fixed to be at the seafloor. The inversion procedure is to search for the optimal fault parameters that give the minimum relative differences (equation (A3) in the supporting information), which are the root-mean-square (RMS) of data model differences divided by RMS of GRACE data. Our inverted uniform slip fault model improves the relative differences with GRACE CSR observation by about 20% as compared with the slip model inverted using GPS and seismic data by *Wei et al.* [2012] and *Ozawa et al.* [2011]. During the inversion, the rake angle quickly converged to its optimal value at $77.0° \pm 2°$ (Table 1). We define the solution uncertainty by using the range (Figure S12), which produces no more than 0.1% of the relative differences (equation (A3) in the supporting information), as compared to the optimal solution during the inversion. The GRACE inverted rake angle is about 10° smaller than most of the published estimates. The smaller rake angle indicates that the azimuth of the slip vector (A4) is about 10° larger than some of the published solutions (Table 1) and it is about 5° larger than the published U.S. Geological Survey centroid moment tensor (USGS CMT) solution (http://earthquake.usgs.gov/earthquakes/eqinthenews/2011/usc0001xgp/neic_c0001xgp_cmt.php), which gives the smaller rake angle than our solution but has a correspondingly small strike angle. The different orientation of our estimated slip model can be explained by the spatial orientation of the observed gravity and gravity gradient changes, which is about 10° clockwise from the model prediction.

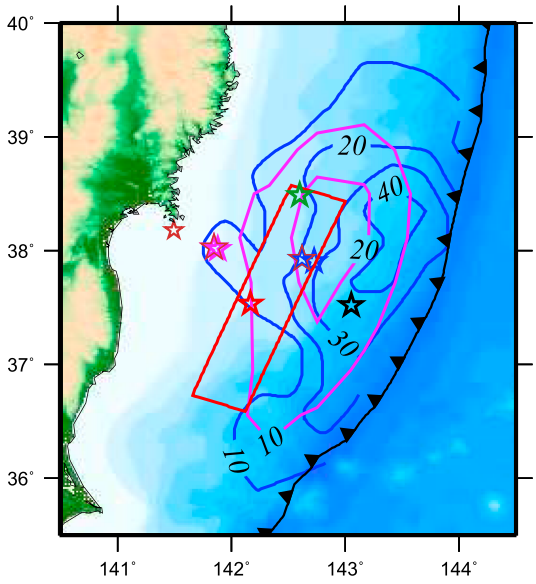

Figure 5. Comparison of slip distribution models. The black triangle line is the plate boundary [*Bird*, 2003]. The black and green stars are the GCMT and USGS CMT estimated centroid locations, respectively. The brown star is the centroid location of postseismic slip model [*Ozawa et al.*, 2011]. The slip contours (m) are from the published coseismic slip models: GPS-only model in magenta [*Ozawa et al.*, 2011] and GPS/seismic model in blue [*Wei et al.*, 2012]. The centroid location of these two slip models are denoted as blue and magenta stars, which are outlined with brown color when combined with the postseismic slip model. The contribution of the postseismic slip to centroid location is negligible as shown that the magenta star and the magenta star with brown outline are almost at the same location. The red star is estimated centroid location with the red rectangle as fault boundary using the GRACE CSR data, which is about 40 km south and 40 km west of the centroid location (blue star) by *Wei et al.* [2012].

The centroid location is well resolved to be at $142.17 \pm 0.05°$E, $37.53 \pm 0.08°$N, shown as a red star in Figure 5. As it is well known, seismic data tend to yield average slip near trench, e.g., the blue contour and blue star [*Wei et al.*, 2012] (Figure 5), and GPS data infer an average slip closer to land, as shown by the magenta contour and magenta star (Figure 5) [*Ozawa et al.*, 2011]. GRACE data resolved location is in between these two other solutions in the west-east direction. Although our solution is about 40 km south of the solutions in *Wei et al.* [2012] and *Ozawa et al.* [2011], it centers at the same latitude as the GCMT centroid, and it is 30 km west of the USGS CMT solution.

The seismic moment converges to its optimal solution well, which is $(6.43 \pm 0.4) \times 10^{22}$ N m (Table 1), corresponding to a *Mw* value of 9.14 ± 0.02, which is larger than estimates of other slip models (Table 1), and can be explained by the larger gravity magnitude as observed by GRACE, considering that the GRACE solution contain the afterslip information in March 2011. Estimated fault width is 70 ± 20 km using GRACE data. However, the resolved fault length has large deviations to make relative difference close to its minimum, which is 240 ± 110 km, indicating that as discussed before, the fault length is relatively hard to be constrained by GRACE data. Since length, width, and slip together determine the signal magnitude, the small width indicates a large slip and the larger deviation in length leads to a larger uncertainty for estimated average slip, which is 127 ± 100 m.

5. Sensitivity of GRACE Data Over Offshore Seismic Deformations

GRACE-observed coseismic gravity change is at much coarser resolution than other geodetic data, namely, GPS or synthetic aperture radar interferometry-measured land displacement. However, GRACE directly observes right above the fault area of the March 2011 Tohoku undersea earthquake, providing a better spatial coverage. Here we further illustrate that GRACE observation provides independent constraints on the earthquake source parameters complementary to the on-land GPS and seismic data. Using both onshore and offshore GPS/Acoustic Network data, *Wang et al.* [2013] obtained a slip model (Model 1) with the maximum slip of ~ 48 m at (38.13°N, 143.26°E, 15.5 km), rake 74° at the peak slip, and an average rake of 80°. Using only the onshore GPS data, they obtained a model (Model 4) with the maximum slip of ~23 m at (38.06°N, 142.80° E, 24.4 km), rake 79° at the peak slip, and an average rake of 83°. Both slip models explain the onshore GPS data equally well, but the slip model using the offshore GPS data has been proven to fit the tsunami observations much better than the model with only onshore GPS data [*Wang et al.*, 2013]. The slip orientation of our model is obviously closer to Model 1 than 4, further demonstrating that the GRACE data are able to provide additional constraint similar to the offshore GPS observation. In addition, the RMS and relative differences (equation (A3) in the supporting information) between the GRACE observation and these two slip model predictions are computed, and the results are shown in Table S1, showing that GRACE is closer to Model 1 than Model 4, with an RMS of 1.5 and 1.6 μGal for g_N, respectively.

6. Conclusions

Our new approach can retrieve significantly more enhanced coseismic gravity change signals. We obtained a peak magnitude of -17.6 ± 1.1 μGal (Figure 2a) for g_N change, larger than previously published values, e.g., than the peak coseismic g_D change of -7 μGal estimated by *Matsuo and Heki* [2011] and than the peak g_D change of -8.75 ± 1.6 μGal estimated by *Wang et al.* [2012b], even though the seismic gravity change of the component g_D is always larger than the change of other two components, including g_N change. Using an elaborate simulated annealing algorithm inversion scheme and the improved GRACE gravity and gravity gradient observations (g_N, *Txx*, *Txy*, and *Txz*), we demonstrated that GRACE data can provide a good constraint to fault seismic moment, fault width, especially for rake angle and centroid location. Our solution produces a centroid location that is close to the latitude of GCMT solution, and the longitude of USGS solution and gives a slip orientation that is about 5°–10° clockwise from published GPS/seismic slip models. Compared to the two slip models given by *Wang et al.* [2013], our slip model is closer to Model 1 that is resolved using both onshore and offshore GPS data than Model 4 which used only onshore GPS data, indicating that GRACE data independently contain reliable signal over the offshore area. However, the question of how the systematic or stochastic error from GRACE data affect the resolved parameters need to be further studied. Nevertheless, our inverted fault model still has around 40% relative difference (39%, 27%, 52%, and 40% for g_N, *Txx*, *Txy*, and *Txz*) using GRACE observations. This may be due to the fact that our uniform dislocation model is too simple to represent the actual fault mechanism, which is a subject for future studies.

Acknowledgments

The Ohio State University component of this research is primarily supported by NASA's Earth and Space Science Fellowship (ESSF) Program (Grant NNX12AO06H), partially supported by NSF Division of Earth Sciences (Grant EAR-1013333), and by the Chinese Academy of Sciences/SAFEA International Partnership Program for Creative Research Teams (Grant KZZD-EW-TZ-05). GRACE data products are from NASA's PODAAC via JPL, CSR, and GFZ. Some figures in this paper were generated using the Generic Mapping Tools (GMT) [*Wessel and Smith*, 1991]. This work was also supported in part by an allocation of computing resources from the Ohio Supercomputer Center (http://www.osc.edu). We acknowledge Frederik Simons for valuable intellectual exchanges and for his open software on localized spectral analysis. We thank Eric Calais and an anonymous reviewer for their helpful comments and Srinivas Bettadpur for useful discussions on GRACE data processing.

The Editor thanks an anonymous reviewer for his/her assistance in evaluating this paper.

References

Ammon, C. J., T. Lay, H. Kanamori, and M. Cleveland (2011), A rupture model of the 2011 off the Pacific coast of Tohoku earthquake, *Earth Planets Space*, *63*, 693–696.

Bassin, C., G. Laske, and G. Masters (2000), The current limits of resolution for surface wave tomography in North America, *EOS Trans AGU*, *81*, F897.

Bird, P. (2003), An updated digital model of plate boundaries, *Geochem. Geophys. Geosyst.*, *4*(3), 1027, doi:10.1029/2001GC000252.

Cambiotti, G., and R. Sabadini (2012), A source model for the great 2011 Tohoku earthquake (*Mw* = 9.1) from inversion of GRACE gravity data, *Earth Planet. Sci. Lett.*, *335–336*, 72–79.

Duan, X. J., J. Y. Guo, C. K. Shum, and W. van der Wal (2009), On the postprocessing removal of correlated errors in GRACE temporal gravity field solutions, *J. Geod.*, *83*, 1095–1106, doi:10.1007/s00190-009-0327-0.
Goffee, W. L., G. D. Ferrier, and J. Rogers (1994), Global optimization of statistical functions with simulated annealing, *J. Econom.*, *60*, 65–99.
Han, S.-C., C. Shum, M. Bevis, C. Ji, and C. Kuo (2006), Crustal dilatation observed by GRACE after the 2004 Sumatra-Andaman earthquake, *Science*, *313*(5787), 658–661.
Han, S.-C., J. Sauber, and S. Luthcke (2010), Regional gravity decrease after the 2010 Maule (Chile) earthquake indicates large-scale mass redistribution, *Geophys. Res. Lett.*, *37*, L23307, doi:10.1029/2010GL045449.
Han, S.-C., J. Sauber, and R. Riva (2011), Contribution of satellite gravimetry to understanding seismic source processes of the 2011 Tohoku-Oki earthquake, *Geophys. Res. Lett.*, *38*, L24312, doi:10.1029/2011GL049975.
Han, S.-C., R. Riva, J. Sauber, and E. Okal (2013), Source parameter inversion for recent great earthquakes from a decade-long observation of global gravity fields, *J. Geophys. Res. Solid Earth*, *118*, 1240–1267, doi:10.1002/jgrb.50116.
Hayes, G. P. (2011), Rapid source characterization of the Mw 9.0 off the Pacific coast of Tohoku earthquake, *Earth Planets Space*, *63*, 529–534, doi:10.5047/eps.2011.05.012.
Heki, K., and K. Matsuo (2010), Coseismic gravity changes of the 2010 earthquake in central Chile from satellite gravimetry, *Geophys. Res. Lett.*, *37*, L24306, doi:10.1029/2010GL045335.
Ji, C., D. J. Wald, and D. V. Helmberger (2002), Source description of the 1999 Hector Mine, California, earthquake, part I: Wavelet domain inversion theory and resolution analysis, *Bull. Seismol. Soc. Am.*, *92*, 1192–1207.
Kirkpatrick, S., C. D. Gelatt Jr., and M. P. Vecchi (1983), Optimization by simulated annealing, *Science*, *220*, 671–680, doi:10.1126/science.220.4598.671.
Lay, T., C. Ammon, H. Kanamori, L. Xue, and M. Kim (2011), Possible large near-trench slip during the 2011 Mw 9.0 off the Pacific coast of Tohoku earthquake, *Earth Planets Space*, *63*, 687–692.
Li, J., and W. B. Shen (2011), Investigation of the co-seismic gravity field variations caused by the 2004 Sumatra-Andaman earthquake using monthly GRACE data, *J. Earth Sci.*, *22*(2), 280–291.
Matsuo, K., and K. Heki (2011), Coseismic gravity changes of the 2011 Tohoku-Oki earthquake from satellite gravimetry, *Geophys. Res. Lett.*, *38*, L00G12, doi:10.1029/2011GL049018.
Ozawa, S., T. Nishimura, H. Suito, T. Kobayashi, M. Tobita, and T. Imakiire (2011), Coseismic and postseismic slip of the 2011 magnitude-9 Tohoku-Oki earthquake, *Nature*, *475*, 373–376, doi:10.1038/nature10227.
Panet, I., F. F. Pollitz, V. Mikhailov, M. Diament, P. Banerjee, and K. Grijalva (2010), Upper mantle rheology from GRACE and GPS postseismic deformation after the 2004 Sumatra-Andaman earthquake, *Geochem. Geophys. Geosyst.*, *11*, Q06008, doi:10.1029/2009GC002905.
Pollitz, F. F., R. Bürgmann, and P. Banerjee (2011), Geodetic slip model of the 2011 M9.0 Tohoku earthquake, *Geophys. Res. Lett.*, *38*, L00G08, doi:10.1029/2011GL048632.
Shao, G., X. Li, C. Ji, and T. Maeda (2011), Focal mechanism and slip history of the 2011 Mw 9.1 off the Pacific coast of Tohoku earthquake, constrained with teleseismic body and surface waves, *Earth Planets Space*, *63*, 559–564, doi:10.5047/eps.2011.06.028.
Simons, F., F. Dahlen, and M. Wieczorek (2006), Spatiospectral concentration on a sphere, *SIAM Rev.*, *48*(3), 504–536, doi:10.1137/S0036144504445765.
Simons, M., et al. (2011), The 2011 magnitude 9.0 Tohoku-Oki earthquake: Mosaicking the megathrust from seconds to centuries, *Science*, *332*, 1421–1425, doi:10.1126/science.1206731.
Swenson, S., and J. Wahr (2006), Post-processing removal of correlated errors in GRACE data, *Geophys. Res. Lett.*, *33*, L08402, doi:10.1029/2005GL025285.
Wang, R., F. Lorenzo-Martin, and F. Roth (2006), PSGRN/PSCMP—A new code for calculating co- and post-seismic deformation, geoid and gravity changes based on the viscoelastic-gravitational dislocation theory, *Comput. Geosci.*, *32*, 527–541, doi:10.1016/j.cageo.2005.08.006.
Wang, L., C. Shum, F. Simons, A. Tassara, K. Erkan, C. Jekeli, A. Braun, C. Kuo, H. Lee, and D. Yuan (2012a), Coseismic slip of the 2010 Mw 8.8 Great Maule, Chile, earthquake quantified by the inversion of GRACE observations, *Earth Planet. Sci. Lett.*, *335–336*, 167–179.
Wang, L., C. Shum, F. Simons, B. Tapley, and C. Dai (2012b), Coseismic and postseismic deformation of the 2011 Tohoku-Oki earthquake constrained by GRACE gravimetry, *Geophys. Res. Lett.*, *39*, L07301, doi:10.1029/2012GL051104.
Wang, L., C. Shum, and C. Jekeli (2012c), Gravitational gradient changes following the 2004 December 26 Sumatra–Andaman earthquake inferred from GRACE, *Geophys. J. Int.*, *191*(3), 1109–1118, doi:10.1111/j.1365-246X.2012.05674.x.
Wang, R., S. Parolai, M. Ge, M. Ji, T. R. Walter, and J. Zschau (2013), The 2011 Mw 9.0 Tohoku-Oki earthquake: Comparison of GPS and strong-motion data, *Bull. Seismol. Soc. Am.*, *103*(2B), 1336–1347, doi:10.1785/0120110264.
Wei, S., R. Graves, D. Helmberger, J. P. Avouac, and J. Jiang (2012), Sources of shaking and flooding during the Tohoku-Oki earthquake: A mixture of rupture styles, *Earth Planet. Sci. Lett.*, *333–334*, 91–100.
Wessel, P., and W. H. F. Smith (1991), Free software helps map and display data, *Eos Trans. AGU*, *72*(41), 441, doi:10.1029/90EO00319.
Wieczorek, M. A., and F. J. Simons (2005), Localized spectral analysis on the sphere, *Geophys. J. Int.*, *162*, 655–675.